Hysteretic thermal spin-crossover and symmetry breaking in heteroleptic Fe(II) complexes using alkyl chain substituted 2,2'-dipyridylamine ligands.

Blaise L. Geoghegan,[a] Wasinee Phonsri,[b] P. N. Horton,[c], J. B. Orton,[c] S. J. Coles,[c] Keith S. Murray,[b] Peter J. Cragg,[a] Marcus K. Dymond[a] and Ian A. Gass[a]*

[a]School of Pharmacy and Biomolecular Sciences, Huxley Building, University of Brighton, Brighton, BN2 4GJ, England, UK.
[b]School of Chemistry, Building 23, Monash University, Clayton, Victoria, Australia.
[c]The UK National Crystallography Service, School of Chemistry, University of Southampton, Southampton, SO17 1BJ, UK.

E-mail: I.Gass@brighton.ac.uk

Abstract

The alkyl chain carrying ligands *N,N*-di(pyridin-2-yl)butanamide (LC_4) and *N,N*-di(pyridin-2-yl)decanamide (LC_{10}) were combined with NCS^- co-ligands to form the neutral heteroleptic Fe(II) complexes *trans*-$[Fe^{II}(LC_4)_2(NCS)_2]$ (**1C$_4$**) and *trans*-$[Fe^{II}(LC_{10})_2(NCS)_2]$ (**1C$_{10}$**). Variable temperature crystallographic studies revealed that **1C$_4$** is in the orthorhombic space group $Pna2_1$ between 85-200 K whereas **1C$_{10}$** is in the monoclinic space group $P2_1/c$ between 85-105 K before undergoing a crystallographic phase transition to the triclinic space group $P\bar{1}$ by 140 K. The average Fe-N bond lengths suggest that at 85 K **1C$_4$** contains LS Fe(II) centres; However, the *ca.* 0.18 Å increase in the average Fe-N bond lengths between 85 and 120 K suggests a spin-transition occurs within this temperature interval and the HS state is predominant beyond this. **1C$_{10}$** contains LS Fe(II) centres between 85 and 105 K. Upon warming from 105 to 140 K the average Fe-N bond lengths increase by *ca.* 0.19 Å, which suggests that a spin-transition to the HS accompanies the $P2_1/c$ to $P\bar{1}$ crystallographic phase transition. Solid-state magnetic susceptibility measurements showed that **1C$_4$** undergoes semi-abrupt spin-crossover with $T_{1/2}$ = 127.5 K and a thermal hysteresis of *ca.* 13 K whereas, **1C$_{10}$** undergoes an abrupt spin-crossover with $T_{1/2}$ = 119.0 K, and is also accompanied by thermal hysteresis of *ca.* 4 K. The crystallographic and magnetic data show that the length of the complex's alkyl chain substituents can have a large impact on the structure of the crystal lattice as well as a subtle effect on the $T_{1/2}$ value for thermal spin-crossover.

Introduction

The spin-crossover[1] (SCO) phenomenon is most commonly encountered in octahedral Fe(II) species where a reversible transition between the quantum mechanical ground state (low-spin (LS) state), and the thermodynamically stable high-spin (HS) state can be achieved by application of external influences such as temperature,[2] pressure,[3] irradiation[4,5] and applied magnetic fields.[6] Cooperative SCO systems rely on strong intermolecular interactions such as hydrogen bonds and $\pi\cdots\pi$ contacts and this cooperativity can result in an abrupt spin-transition often accompanied by thermal hysteresis. This enables bistability between the two spin states, making SCO materials ideal candidates for use as switches or memory devices. This transition between the LS and HS states, with a subsequent change in the Fe(II) to ligand donor atom distance, results in a significant change in the material's magnetic and electric dipole moments, conductivity and optical properties.[7,8] This makes SCO materials attractive targets for both molecular-based spintronic devices[9–11] and hybrid multifunctional materials incorporating a secondary function such as luminescence or chirality.[12]

In 2005 Réal and co-workers investigated Fe(II) complexes of di(pyridin-2-yl)amine (dpa), and showed that *cis*-$[Fe^{II}(dpa)_2(NCS)_2]$ underwent gradual and incomplete thermal SCO with a $T_{1/2}$ value of 88 K.[13] This $T_{1/2}$ value and nature of the spin transition can be changed by modification of the amine group of the dpa ligand with notable examples including derivatised dpa/triazine ligands including: *trans*-$[Fe^{II}(DPT)_2(NCS)_2]\cdot CH_3OH$ which undergoes a gradual incomplete spin-transition with $T_{1/2}$ of 150 K;[14] α-*trans*-$[Fe^{II}(DBB)_2(NCS)_2]$ exhibiting a complete abrupt spin-transition ($T_{1/2}$ = 170 K);[15] β-*trans*-$[Fe^{II}(DBB)_2(NCS)_2]$ showing a gradual but complete spin transition ($T_{1/2}$ = 300 K);[15] and *trans*-$[Fe^{II}(Cladpat)_2(NCS)_2]$ undergoing a complete spin transition with a $T_{1/2}$ value of 178 K[16] (DPT = 6-phenoxy-N^2,N^2,N^4,N^4-tetra-2-

pyridinyl-1,3,5-triazine-2,4-diamine; DBB= (N^2,N^2,N^4,N^4-tetrabenzyl-N^6,N^6-di(pyridin-2-yl)-1,3,5-triazine-2,4,6-triamine; and Cladpat = 6-chloro-N'-phenyl-*N*,*N*-di(pyridin-2-yl)-1,3,5-triazine-2,4-diamine). The work outlined above set a precedent for investigation of Fe(II) systems that incorporate derivatised dpa ligands and NCX co-ligands (where X = is typically S, Se, BH_3) in an attempt to tailor the magnetic properties of the resultant materials. This approach allows for the possibility of multifunctionality through selection of a desirable *N*-substituent, such as alkyl chains, on to the parent dpa scaffold.

A number of studies have focussed on utilising the conformational changes of alkyl chain containing materials to: probe the relationship between SCO and thermotropic liquid crystal behaviour;[17–20] develop dual functioning SCO-active materials such as those found in Langmuir-Blodgett films;[21] and study biomimetic models of phospholipid membranes. [22,23] A recent example by Clérac *et al*. of an iron(II) complex functionalised with decyl alkyl chains, [Fe(C_{10}-pbh)$_2$] (C_{10}-pbh = (1*Z*,*N*′*E*)-4-(decyloxy)-*N*′-(pyridin-2-ylmethylene)-benzohydrazonate)), had a SCO transition with a 35 K thermal hysteresis near room temperature with phase dependent magnetic properties.[24] It is encouraging that the alkyl chain component of such materials does not necessarily inhibit any desirable SCO properties such as abrupt/hysteretic spin-transitions and cooperative lattice effects.[25–29] Here we report a family of SCO-active, mononuclear, neutral complexes of Fe(II) based on the alkyl chain containing ligands *N,N*-di(pyridin-2-yl)butanamide (LC_4) and *N,N*-di(pyridin-2-yl)decanamide (LC_{10}) (Scheme 1) with formula [$Fe^{II}(LC_x)_2(NCS)_2$] where x = 4 (**1C$_4$**) or 10 (**1C$_{10}$**).

Experimental

General

All reagents were purchased from Sigma-Aldrich (Merck) and were used as received without further purification. All solvents were purchased from Fisher Scientific. Methanol was dried over 4 Å molecular sieves (20% w/w) for a minimum period of 48 h before use in synthetic procedures. All synthetic procedures were done under aerobic conditions unless otherwise stated. ^{1}H and ^{13}C NMR spectra were recorded in deuterochloroform ($CDCl_3$) containing 1% trimethylsilane (TMS) on a Bruker Avance 400 MHz spectrometer and can be found in Figs S18-S25. The following abbreviations are used for the multiplicities: s = singlet, d = doublet, t = triplet, q = quartet, quin = quintuplet, sext = sextet and m = multiplet. Mass spectrometry was collected on a bruker MicroTOF instrument with positive mode electrospray ionisation and using methanol as the eluent (Fig. S26 and S27). A Perkin Elmer Spectrum 65 FT spectrophotometer was used to obtain IR data at room temperature and UV-Vis spectra were recorded performed on a Shimadzu UV-2401PC spectrophotometer in acetone.

Elemental analysis

Elemental analysis was obtained by MEDAC LTD analytical and chemical consultancy service.

X-ray crystallography

X-ray crystallography was conducted on a sample of fresh single crystals of **$1C_4$** and **$1C_{10}$**. The single crystal was selected from a vial containing the methanolic mother liquor under a nitrogen atmosphere and placed straight into oil to avoid drying. Variable temperature X-ray diffraction data for **$1C_4$** were collected using an AFC12 goniometer and a HyPix-600HE

detector, FR-E+ SuperBright Molybdenum X-Ray generator and a highly focused beam (70µm) achieved with VariMax VHF optics. The diffractometers were also equipped with the Oxford Cryosystems Cobra. Variable temperature X-ray diffraction data for **$1C_{10}$** were collected using an AFC12 goniometer and a HyPix-600HE detector, FR-E+ SuperBright Molybdenum X-Ray generator and a highly focused beam (70µm) achieved with VariMax VHF optics. **$1C_4$·85K** was solved using intrinsic phasing and refined by full-matrix least-squares on F^2 with SHELXL.[30] **$1C_4$·120K** was solved and refined using Olex2[31,32] and **$1C_4$·200 K** was solved using Olex2[32] and refined by full-matrix least-squares on F^2 with SHELXL.[30] **$1C_{10}$·85K**, **$1C_{10}$·105K** and **$1C_{10}$·140K** were solved using direct methods with SHELXS[33] and refined by full-matrix least-squares on F^2 with SHELXL.[30] Crystallographic and refinement parameters; selected bond length and angles; and selected intermolecular contact distances for all the crystal structures are located in Tables 1-6 and Table S1. CCDC 1947560-1947565 contains the supplementary crystallographic data for this paper. The data can be obtained free of charge from The Cambridge Crystallographic Data Centre via www.ccdc.cam.ac.uk/structures.

Magnetic Susceptibility Measurements

Variable-temperature magnetic susceptibility measurements were performed on a Quantum Design MPMS 7T SQUID magnetometer over the temperature range 50-340 K at a 5 K min^{-1} rate for **$1C_4$** and **$1C_{10}$** under an applied field of 0.1 T. The crystals of **$1C_4$** and **$1C_{10}$** were in methanol under a nitrogen atmosphere but were filtered, air dried quickly and then encased in Vaseline to avoid any torqueing effects. These samples were held in a capsule at the centre of a drinking straw fixed to the sample rod. The magnetometer was calibrated by either a standard palladium sample or $CuSO_4 \cdot 5H_2O$ and diamagnetic corrections were applied using

Pascal's constants. The molecular weight used in the magnetic measurements were based on the solvated forms of **1C$_4$** and **1C$_{10}$** as defined by the microanalysis (**1C$_4$·2H$_2$O** and **1C$_{10}$·H$_2$O**).

Synthetic procedures

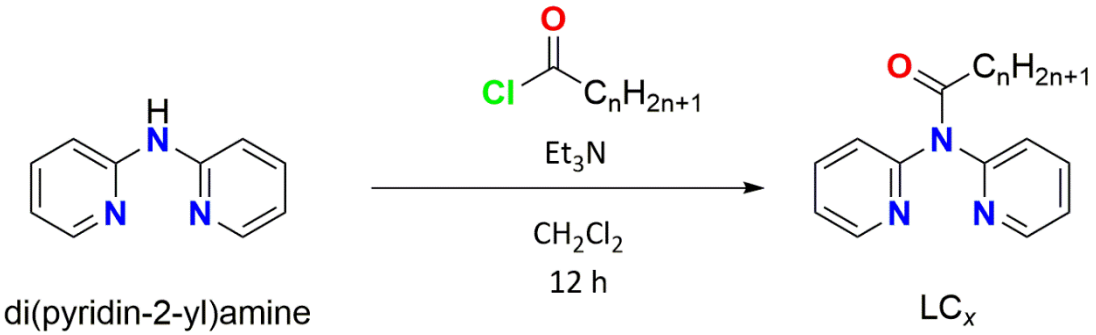

Scheme 1 Synthetic route to ligands LC$_x$ ligands from di(pyridin-2-yl)amine (dpa), where C$_x$ is the number of carbon atoms in the alkyl chain substituent including that of the carbonyl group.

***N,N*-Di(pyridin-2-yl)butanamide (LC$_4$):** Di(pyridin-2-yl)amine (dpa) (1.712 g, 10 mmol) and triethylamine (Et$_3$N) (2.65 cm^3, 19 mmol) were dissolved in 10 cm^3 of CH$_2$Cl$_2$, cooled over an ice bath and placed under an atmosphere of N$_2$. Butyryl chloride (1.03 cm^3, 10 mmol) was dissolved in 10 cm^3 of CH$_2$Cl$_2$ and added to the dpa/Et$_3$N solution via syringe. The resulting solution was stirred for 12 h under N$_2$. 50 cm^3 of a saturated aqueous ammonium chloride solution was added to the reaction solution and the organic phase was separated. The aqueous phase was then extracted with 2 x 20 cm^3 of CH$_2$Cl$_2$ and the organic extracts combined. The combined organic phases were then extracted with 3 x 30 cm^3 of a 10% (w/v) aq. NaCl solution. The organic phase was then washed firstly with 50 cm^3 of 0.1 M aq. NaOH and finally 50 cm^3 of 0.1 M aq. HCl solution before the organic phase was dried over anhydrous MgSO$_4$. This solution was then gravity filtered and the solvent evaporated under reduced pressure to afford LC$_4$ as a pale orange solid. Yield = 1.86 g, 7.7 mmol (77%). ^{1}H NMR

($CDCl_3$, 400 MHz) δ: 8.45 (ddd, *J* = 4.9, 2.0, 0.7 Hz, 2H), 7.76 (td, *J* = 7.8, 2.0 Hz, 2H), 7.51 (d, *J* = 8.1 Hz, 2H), 7.19 (ddd, *J* = 7.5, 4.8, 1.0 Hz, 2H), 2.29 (t, *J* = 7.3 Hz, 2H), 1.70 (sext, *J* = 7.6 Hz, 2H), 0.91 (t, *J* = 7.4 Hz, 3H). ^{13}C NMR ($CDCl_3$, 100 MHz) δ: 173.7, 154.8, 149.0, 138.0, 122.3, 121.9, 38.1, 18.5, 13.7, MS (ESI^+) (MeOH): *m/z* calcd for $C_{14}H_{15}N_3O$ $[M]^+$, 241.29; found, 264.07 $[M + Na]^+$, 505.17 $[2M + Na]^+$.

***N,N*-Di(pyridin-2-yl)decanamide (LC_{10}):** LC_{10} was prepared via the same procedure as LC_4, using decanoyl chloride (2.08 cm^3, 10 mmol). The compound was afforded as a yellow-brown solid. Yield = 2.44 g, 7.5 mmol (75%). ^{1}H NMR ($CDCl_3$, 400 MHz) δ: 8.45 (ddd, *J* = 4.9, 2.0, 0.7 Hz, 2H), 7.76 (td, *J* = 7.8, 2.0 Hz, 2H), 7.51 (d, *J* = 8.1 Hz, 2H), 7.18 (ddd, *J* = 7.5, 4.8, 1.0 Hz, 2H), 2.30 (t, *J* = 7.4 Hz, 2H), 1.66 (quin, *J* = 7.5, 7.0 Hz, 2H), 1.23 (m, 12H), 0.87 (t, *J* = 7.2 Hz, 3H). ^{13}C NMR ($CDCl_3$, 100 MHz) δ: 173.7, 154.8, 148.9, 138.5, 122.4, 121.8, 36.3, 31.8, 29.4, 29.3, 29.2, 25.1, 22.6, 14.0. MS (ESI^+) (MeOH): *m/z* calcd for $C_{20}H_{27}N_3O$ $[M]^+$, 325.46; found, 326.2 $[M + H]^+$, 349.20 $[M + Na + H]^+$, 364.20 $[M + K]^+$.

$[Fe^{II}(LC_4)_2(NCS)_2]$ ($1C_4$): $Fe(BF_4)_2{\cdot}6H_2O$ (33.8 mg, 0.1 mmol) and ascorbic acid (5 mg, 0.003 mmol) were placed into a 10 cm^3 round bottomed flask, dissolved in 2 cm^3 of dry methanol and placed under a nitrogen atmosphere. LC_4 (48.2 mg, 0.2 mmol) was added to a second 10 cm^3 round bottomed flask, dissolved in 2 cm^3 of dry methanol and placed under a nitrogen atmosphere. KSCN (19.4 mg, 0.2 mmol) was added to the solution of $Fe(BF_4)_2{\cdot}6H_2O$ and ascorbic acid, which was subsequently left for 10 min. Next, the solution containing the $Fe(BF_4)_2{\cdot}6H_2O$ was transferred via syringe to the solution containing LC_4. After 12 h, single crystals of **$1C_4$** had formed. For microanalysis, infrared measurements and yield calculations these crystals were collected via glass pipette and placed onto filter paper, quickly dried in air and then placed in a 20 cm^3 glass vial and purged with nitrogen gas. Although the single crystal used for X-ray diffraction studies was found to be solvate free (see below) the air-dried

crystals had acquired two water solvates, affording **$1C_4 \cdot 2H_2O$**. Elemental analysis (air-dried crystals) found: C, 51.91; H, 4.38; N, 16.28. Calc. for $C_{30}H_{30}FeN_8O_2S_2 \cdot 2H_2O$: C, 52.17; H, 4.96; N, 16.23 %. IR (air-dried crystals) ν_{max} (cm^{-1}) 3077vw, 2961w, 2868w, 2045vs, 1693vs, 1600s, 1565m, 1481s, 1463vs, 1438vs, 1378s, 1316vs, 1238vs, 1198vs, 1157s, 1101s, 1057m, 1017s, 970w, 886m, 802s, 783m, 765s, 690m, 650m.

$[Fe^{II}(LC_{10})_2(NCS)_2]$ ($1C_{10}$): $1C_{10}$ was prepared via the same procedure as **$1C_4$**, using LC_{10} (65.1 mg, 0.2 mmol) and all subsequent measurements performed in a similar way. The single crystal used for the X-ray diffraction studies was solvate free whereas the air-dried crystals had acquired one water solvate molecule, affording **$1C_{10} \cdot H_2O$**. Elemental analysis (air dried crystals) found: C, 59.58; H, 6.55; N, 13.24. Calc. for $C_{42}H_{54}FeN_8O_2S_2 \cdot H_2O$: C, 59.99; H, 6.71; N, 13.33 %.IR (air-dried crystals) ν_{max} (cm^{-1}) 3077vw, 2961w, 2868w, 2045vs, 1693vs, 1600s, 1565m, 1481s, 1463vs, 1438vs, 1378s, 1316vs, 1238vs, 1198vs, 1157s, 1101s, 1057m, 1017s, 970w, 893vw, 802s, 783m, 765s, 690m, 650m.

Results and Discussion

Variable temperature crystallographic studies

Structural description of $1C_4$·85K, $1C_4$·120K and $1C_4$·200K.

Table 1 Crystallographic parameters and refinement details for **$1C_4$·85K**, **$1C_4$·120K**, **$1C_4$·200K**.

Parameters	**$1C_4$·85K**	**$1C_4$·120K**	**$1C_4$·200K**
Formula	$C_{30}H_{30}FeN_8O_2S_2$	$C_{30}H_{30}FeN_8O_2S_2$	$C_{30}H_{30}FeN_8O_2S_2$
M_r	654.59	654.59	654.59
Cryst syst	orthorhombic	orthorhombic	orthorhombic
Space group	$Pna2_1$	$Pna2_1$	$Pna2_1$
a / Å	17.4656(18)	17.2689(10)	17.3108(10)
b / Å	8.3066(6)	8.5587(4)	8.6178(4)
c / Å	20.8857(16)	21.2446(12)	21.2607(14)
α / °	90	90	90
β / °	90	90	90
γ / °	90	90	90
V / Å^3	3030.1(4)	3139.9(3)	3171.7(3)
T / K	85	120	200
Z	4	4	4
ρ_{calcd} / g.cm^{-3}	1.435	1.3846	1.371
λ / Å	0.71073	0.71073	0.71073
No. of indep reflns	6392	7154	6892
No. reflns with $I > 2\sigma(I)$	3826	4326	4113
No. of params	390	390	390
No. of restraints	0	0	0
Final R1[a], wR2[b], ($I > 2\sigma(I)$)	0.0617, 0.1044	0.0551, 0.1244	0.0540, 0.0873
R1[a], wR2[b] (all data)	0.1375, 0.1250	0.0888, 0.1073	0.1234, 0.1043
Goodness of fit	1.0080	1.0098	1.0070
Largest residuals / e Å^{-3}	0.4110	0.7309	0.3370

[a] $R1 = \sum\left||F_0|-|F_c|\right| / \sum F_0$, [b] $wR2=\left\{\sum [w(F_0^2 \sum F_c^2)^2] / \sum [w(F_0^2)]\right\}^{1/2}$

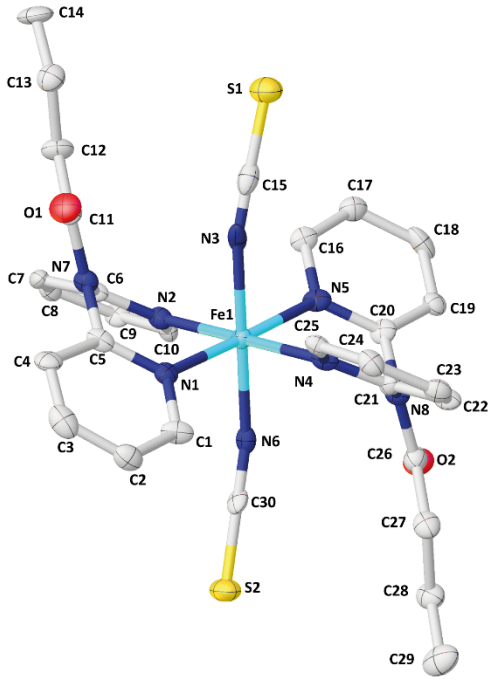

Fig. 1 Molecular structure of **1C$_4$·85K** with atom labels. Hydrogen atoms omitted for clarity. Legend: iron, turquoise; nitrogen, blue; carbon, grey; oxygen, red; sulfur, yellow.

Variable temperature crystallography at 85K (**1C$_4$·85K**), 120 K (**1C$_4$·120K**) and 200 K (**1C$_4$·200K**) were performed on the same single crystal. **1C$_4$·85K**, **1C$_4$·120K** and **1C$_4$·200K** are all in the orthorhombic space group *Pna*2$_1$ with the asymmetric unit containing one complete *trans*-[Fe^{II}(LC$_4$)$_2$(NCS)$_2$] molecule (Table 1). The neutral, heteroleptic complex is formed by two bidentate chelating LC$_4$ ligands in equatorial positions and two NCS$^-$ anions in the *trans* axial sites to form a slightly distorted octahedron with an FeN$_6$ core (Fig. 1). The unit cell of **1C$_4$·85K** is depicted in Fig. S1. The two LC$_4$ ligands coordinate via the pyridyl nitrogen atoms (N1, N2, N4 and N5) and the NCS$^-$ ligands coordinate through the N atom of the nitrile groups (N3 and N6). A selection of bond lengths and angles for the three crystal structures can be found in Table 2. There is evidence of a spin-transition between 85 K and 120 K with **1C$_4$·85K** and **1C$_4$·120K** having average Fe-N bond lengths of 1.994 and 2.178 Å respectively (Table 2);

typical values for an Fe(II) ion undergoing a LS to HS spin-transition.[4,16,27,34,35] In **1C$_4$·200K** the Fe-N bond lengths are similar to that of **1C$_4$·120K**, suggesting the presence of a central HS Fe(II) ion (Table 2).

Table 2 Selected angles and bond lengths for **1C$_4$·85K**, **1C$_4$·120K** and **1C$_4$·200K**.

	1C$_4$·85K	**1C$_4$·120K**	**1C$_4$·200K**
Lengths (Å)			
Fe1-N1	1.999(8)	2.207(4)	2.179(7)
Fe1-N2	2.007(8)	2.181(5)	2.216(5)
Fe1-N3	1.984(8)	2.157(4)	2.144(7)
Fe1-N4	1.995(8)	2.193(4)	2.199(5)
Fe1-N5	1.986(9)	2.207(4)	2.185(6)
Fe1-N6	1.994(10)	2.122(4)	2.119(6)
Fe-N (av.)	1.994	2.178	2.174
Angles (°)			
N1-Fe1-N2	86.4(3)	83.12(15)	83.0(2)
N1-Fe1-N3	89.9(3)	89.47(14)	91.3(2)
N1-Fe1-N4	94.0(3)	98.85(15)	95.4(2)
N1-Fe1-N5	178.7(4)	176.99(16)	178.4(3)
N1-Fe1-N6	88.9(3)	88.73(14)	90.8(2)
N2-Fe1-N3	94.4(3)	90.88(16)	89.6(2)
N2-Fe1-N4	178.5(4)	178.0(2)	177.3(2)
N2-Fe1-N5	92.7(3)	95.11(15)	98.6(2)
N2-Fe1-N6	87.0(3)	90.96(17)	88.4(2)
N3-Fe1-N4	87.1(3)	88.95(15)	88.2(2)
N3-Fe1-N5	89.1(3)	88.13(14)	88.7(2)
N3-Fe1-N6	178.2(4)	177.26(18)	177.0(3)
N4-Fe1-N5	86.9(3)	82.91(16)	83.0(2)
N4-Fe1-N6	91.6(3)	89.29(16)	93.8(2)
N5-Fe1-N6	92.0(3)	93.74(15)	89.3(2)
Fe1-N3-C15 (Fe-NCS)	156.3(7)	145.5(4)	145.9(6)
Fe1-N6-C30 (Fe-NCS)	156.0(8)	147.1(4)	148.8(6)
Σ^a (°)	29.4	39.0	39.7

[a] Octahedral distortion parameters are obtained using the equation: $\Sigma = \sum_{i=1}^{12}(|90-\theta_i|)$, ($\theta_i$ = N-Fe-N) where perfect octahedrons produce a value Σ = 0° and deviation from this value coincides with structural deformation of the coordination polyhedron.

1C$_4$·85K has a distorted octahedral geometry, with an associated octahedral distortion parameter Σ = 29.4°. The spin transition in the Fe(II) ions between 85-120 K is accompanied by further deformation of the FeN_6 polyhedron. This is demonstrated by the increase in the parameter Σ to 39.0° in **1C$_4$·120K** and 39.7° in **1C$_4$·200K**.[5,35,36] The lack of structural transformation between the 120 and 200 K structures of **1C$_4$** suggests that the spin transition is mostly complete by 120 K and the vast majority of the Fe(II) centres will be in the thermodynamically stable HS state.

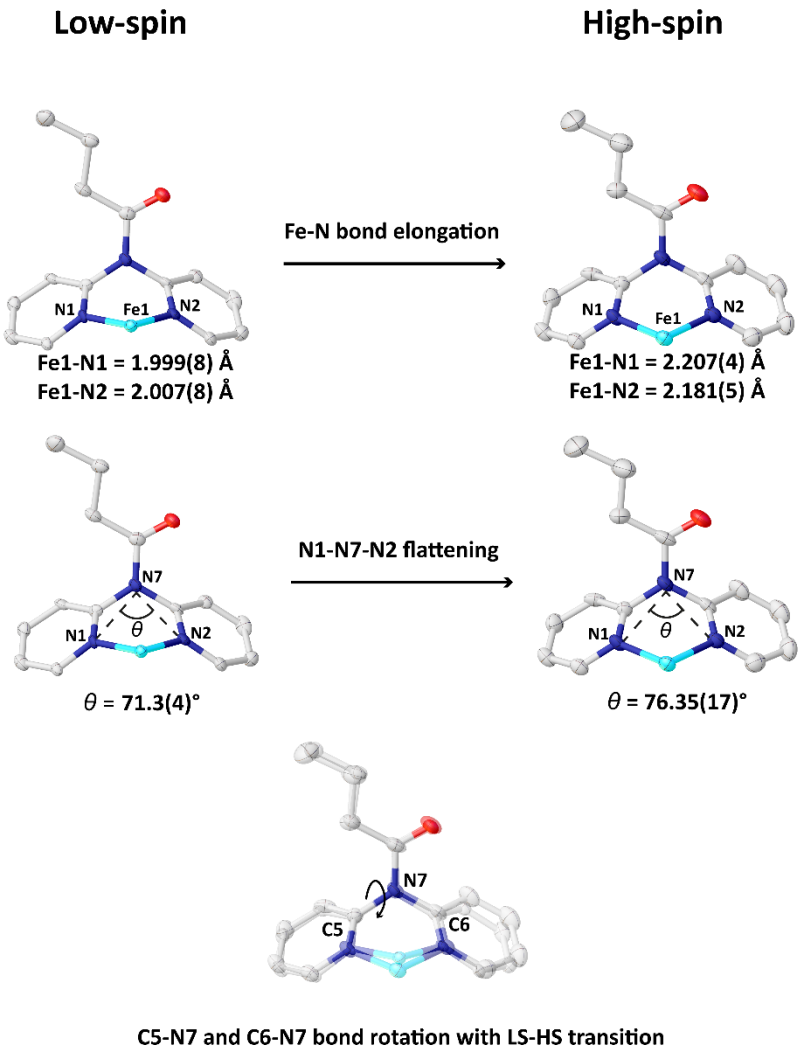

Fig. 2 Structural changes in the LC_4 ligands as the LS to HS conversion takes place in a single crystal of **1C$_4$·85K** (left) and **1C$_4$·120K** (right).

The LC_4 and NCS^- ligands also distort to accommodate the spin transition (Fig. 2). The pyridyl moieties of the ligands rotate about their free axis with the bridging N7 and N8 atoms to accommodate the increasing Fe-N distances for the HS Fe(II) ions. This is manifested by a decrease in the N1-N7-N2 and N4-N8-N5 angles for each ligand unit (Fig. 2). For **1C₄·85K** the N1-N7-N2 angle is 71.3(4)°, rising to 76.4(2)° in **1C₄·120K**, whilst the N1-Fe1-N2 angle in **1C₄·85K** is 86.4(3)° and decreases to 83.1(2)° in **1C₄·120K**. In **1C₄·200K** the angles reported above are similar to that in **1C₄·120K** (N1-N7-N2 = 76.5(3)° and N4-N8-N5 = 76.0(3)°). The Fe-N-C angles, between the central Fe(II) ion and the coordinated SCN group, in **1C₄·85K** are 156.0(8) and 156.3(7)° whereas in **1C₄·120K** these angles decrease to 145.5(4) and 147.1(4)°, to accommodate the change in spin state, which is a common feature noted by Brooker et al.[37] In **1C₄·200K** the Fe-N-C angles remain similar to that in **1C₄·120K** with values of 145.9(6) and 148.8(6)° (Table 2).

Table 3 Selected intermolecular contact distances for **1C₄**.

	1C₄·85K	**1C₄·120K**	**1C₄·200K**
$\pi\cdots\pi$ (Å)[a]	3.500(5)	3.557(3)	3.589(4)
O···C (Å)	3.138(11)	3.116(6)	3.127(9)
O···H-C (°)	126.6(6)	122.5(1)	124.0(5)
Fe···Fe (Å)[b]	8.3066(6)	8.5587(4)	8.6178(4)

[a] Minimum pyridyl centroid···centroid distance. [b] Minimum distance between Fe atoms.

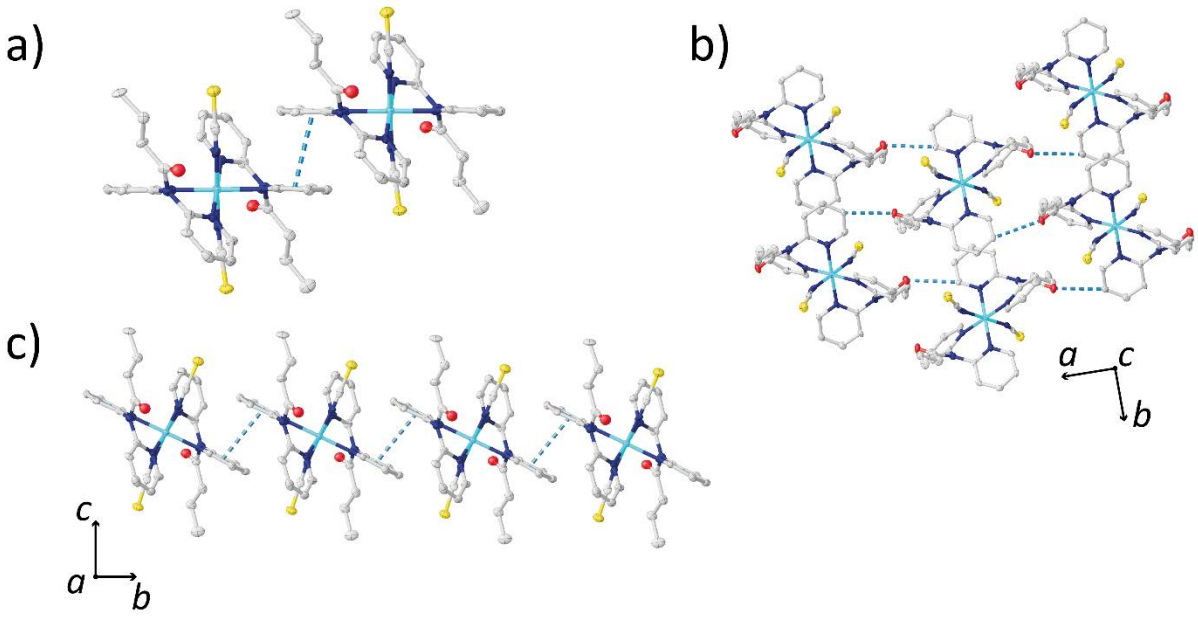

Fig. 3 a) The centroid···centroid $\pi\cdots\pi$ contact between pyridyl groups of **1C$_4$**. b) 2D sheet of short C-H···O contacts in the *ab* plane between complexes of **1C$_4$**. c) 1D chain of complexes of **1C$_4$·85K** as viewed along the *a* axis. These are representative of the similar interactions seen in **1C$_4$·120K** and **1C$_4$·200K**. Legend: iron, turquoise; nitrogen, blue; carbon, grey; oxygen, red; sulfur, yellow.

Neutral complexes of **1C$_4$·85K** pack via short $\pi\cdots\pi$ contacts between nearby pyridyl moieties, resulting in 1D "chains" of complexes propagating along the *b* axis (Fig. 3a and c). The pyridyl groups of the complexes approach each other in a slightly staggered manner and the associated centroid···centroid distance for **1C$_4$·85K** is 3.500(5) Å with the pyridyl groups tightly packed along the *b* axis. This $\pi\cdots\pi$ contact distance gets larger as we increase temperature, with values changing from 3.500(5) Å in **1C$_4$·85K** to 3.557(3) Å in **1C$_4$·120K** and 3.589(4) Å in **1C$_4$·200K** (Table 3). This results in a diagonal expansion of these 1D chains of complexes along the *bc* plane with a subsequent increase in the unit cell parameters *b* and *c* and a concomitant decrease in *a*. In all of the structures there are short C-H···O contacts between the oxygen

atoms of the carbonyl moieties of the LC_4 ligands and the pyridyl C-H groups of a nearby complex (Fig. 3b).[38,39] These C-H···O contacts range from 3.138(11) Å in **1C₄·85K** to 3.116(6) Å in **1C₄·120K** and 3.127(9) Å in **1C₄·200K**. The packing mode of the complexes at all temperatures is almost identical to that of **1C₄·85K** apart from the slightly larger intermolecular distances detailed in Table 3; expected given the spin-transition from LS to HS over this temperature range. The C-H···O contacts propagate across the *ab* plane, and in combination with the 1D $\pi\cdots\pi$ contacts along the *b* axis, form 2D networks of complexes across this crystallographic plane. The alkyl chain tails from each complex extend away from the metal centre in each direction predominantly along the *c* axis. 2D sheets of complexes then stack up the *c* axis and interdigitate their alkyl chain tails to form small regions of hydrophobicity containing aliphatic tails (Fig. 4).

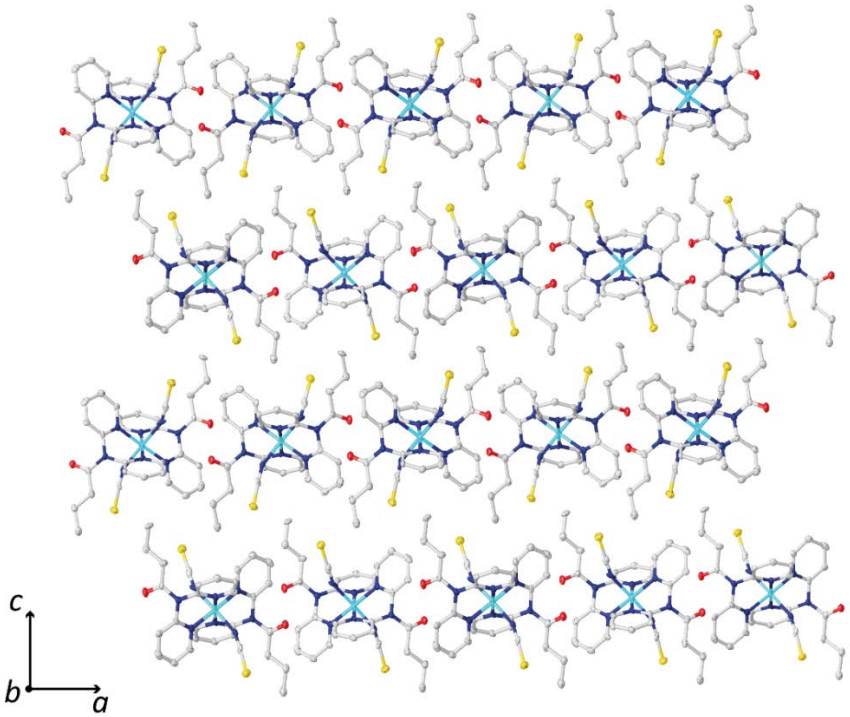

Fig. 4 Packing of **1C₄** at 85 K as viewed down the *b* axis. Hydrogen atoms omitted for clarity. Legend: iron, turquoise; nitrogen, blue; carbon, grey; oxygen, red; sulfur, yellow.

Structural description of $1C_{10}$·85K, $1C_{10}$·105K and $1C_{10}$·140K.

Table 4 Crystallographic parameters and refinement information for **$1C_{10}$·85K**, **$1C_{10}$·105K** and **$1C_{10}$·140K**.

Parameters	**$1C_{10}$·85K**	**$1C_{10}$·105K**	**$1C_{10}$·140K**
Formula	$C_{42}H_{54}FeN_8O_2S_2$	$C_{42}H_{54}FeN_8O_2S_2$	$C_{42}H_{54}FeN_8O_2S_2$
M_r	822.90	822.90	822.90
Cryst syst	monoclinic	monoclinic	triclinic
Space group	$P2_1/c$	$P2_1/c$	$P\bar{1}$
a / Å	15.9053(5)	15.9129(9)	17.4294(5)
b / Å	8.2351(2)	8.2544(3)	18.1352(5)
c / Å	17.5640(4)	17.5843(9)	23.3965(5)
α / °	90	90	74.927(2)
β / °	115.073(3)	114.966(7)	73.006(2)
γ / °	90	90	67.722(3)
V / Å^3	2083.78(11)	2093.9(2)	6450.7(3)
T / K	85	105	140
Z	2	2	6
ρ_{calcd} / g.cm^{-3}	1.312	1.305	1.271
λ / Å	0.71073	0.71073	0.71073
No. of indep reflns	4789	4816	29526
No. reflns with $I > 2\sigma(I)$	4300	4156	10256
No. of params	251	251	1495
No. of restraints	0	0	0
Final R1[a], wR2[b], ($I > 2\sigma(I)$)	0.0278, 0.0682	0.0348, 0.0805	0.0582, 0.1134
R1[a], wR2[b] (all data)	0.0327, 0.0702	0.0434, 0.0843	0.1506, 0.1433
Goodness of fit	1.047	1.034	1.024
Largest residuals / e Å^{-3}	0.368	0.475	0.410

[a] $R1 = \sum \left| |F_0| - |F_c| \right| / \sum F_0$, [b] $wR2 = \left\{ \sum [w(F_0^2 \sum F_c^2)^2] / \sum [w(F_0^2)] \right\}^{1/2}$

Variable temperature crystallography was performed at 85K (**$1C_{10}$·85K**), 105 K (**$1C_{10}$·105K**) and 140 K (**$1C_{10}$·140K**) on the same single crystal of **$1C_{10}$** in a similar vein to that reported above for **$1C_4$**. **$1C_{10}$·85K** and **$1C_{10}$·105K** are in the monoclinic space group $P2_1/c$ but **$1C_{10}$·140K** is in the triclinic space group $P\bar{1}$ indicating that a crystallographic phase transition has taken place between 105 and 140 K (Table 4). The *trans*-$[Fe^{II}(LC_{10})_2(NCS)_2]$ molecular structure of the complex is similar to that of **$1C_4$** (Figs. S2-4) with an identical coordination sphere and steric

arrangement of the ligands, differing only in the length of the alkyl chain tail. In **1C$_{10}$·85K** and **1C$_{10}$·105K** the asymmetric unit contains one half of the molecular unit, with an inversion centre located on the central Fe(II) ion whereas the asymmetric unit of **1C$_{10}$·140K** contains three total molecular units, made up of two whole and two half complete molecular units. The unit cells for **1C$_{10}$·85K**, **1C$_{10}$·105K** and **1C$_{10}$·140K** are shown in Figs. S5, S6 and S7, respectively. Selected bond lengths and angles for all four Fe(II) centres in **1C$_{10}$·140K** are located in Table S1. It is clear that the central Fe(II) ion is low-spin in **1C$_{10}$·85K** and **1C$_{10}$·105K**, with average Fe-N bond lengths of 1.979 and 1.982 Å respectively (Table 5). The significantly larger average Fe-N bond length of 2.172 Å found in **1C$_{10}$·140K** (across all four independent Fe(II) centres. See Table S1) suggests that the system is completely HS at 140 K and that a relatively abrupt spin-transition between 105 K and 140 K must occur. This must be accompanied by a crystallographic phase transition from $P2_1/c$ to $P\bar{1}$ (see below) and this type of transition is often observed in systems that undergo abrupt thermal SCO.[24,40,41] The molecular units of **1C$_{10}$·85K**, **1C$_{10}$·105K** and **1C$_{10}$·140K** have a distorted octahedral geometry with Σ = 28.4°, 28.5° and 35.9°(av.) respectively, supporting the conclusion of a spin-transition between 105 K and 140 K.

The packing in **1C$_{10}$·85K** and **1C$_{10}$·105K** is directed by the same short contacts as **1C$_4$** (Table 6). Intermolecular $\pi\cdots\pi$ contacts along the *b* axis are 3.5670(10) and 3.5770(13) Å (Fig. S8) and the shortest C-H···O contacts are 3.115(1) and 3.121(2) Å for **1C$_{10}$·85K** and **1C$_{10}$·105K**, respectively (Table 6). The similarity in packing between the LS structures of **1C$_{10}$·85K** and **1C$_{10}$·105K** is expected and the 2D networks of complexes formed through the intermolecular contacts are separated by their *trans* alkyl chain tails, which extend mostly down the *a* axis to form layers in the *bc* plane, where the 2D sheets of complexes are between two regions of hydrophobic alkyl chains (Fig. 5).

Table 5 Selected bond lengths and angles for **1C$_{10}$·85K**, **1C$_{10}$·105K** and **1C$_{10}$·140K**.

	1C$_{10}$·85K	**1C$_{10}$·105K**		**1C$_{10}$·140K**[a]
Lengths (Å)			Lengths (av.) (Å)	
Fe1-N1	1.996(1)	1.997(1)	Fe1-N1	2.208
Fe1-N2	1.979(1)	1.983(1)	Fe1-N2	2.188
Fe1-N3	1.963(1)	1.965(1)	Fe1-N3	2.118
Fe1-N1′	1.996(1)	1.997(1)	Fe1-N4	2.187
Fe1-N2′	1.979(1)	1.983(1)	Fe1-N5	2.220
Fe1-N3′	1.963(1)	1.965(1)	Fe1-N6	2.116
Fe-N (av.)	1.979	1.982	Fe-N (av.)	2.173
Angles (°)			Angles (av.) (°)	
N1-Fe1-N2	87.00(4)	86.98(5)	N1-Fe1-N2	83.44
N1-Fe1-N3	86.92(4)	93.15(5)	N1-Fe1-N3	90.31
N1-Fe1-N1′	180.00	180.00	N1-Fe1-N4	96.52
N1-Fe1-N2′	93.00(4)	93.02(5)	N1-Fe1-N5	179.86
N1-Fe1-N3′	86.92(4)	86.85(5)	N1-Fe1-N6	89.70
N2-Fe1-N3	86.92(4)	90.96(5)	N2-Fe1-N3	89.25
N2-Fe1-N1′	93.00(4)	93.02(5)	N2-Fe1-N4	179.94
N2-Fe1-N2′	180.00	180.00	N2-Fe1-N5	96.64
N2-Fe1-N3′	88.98(4)	89.04(5)	N2-Fe1-N6	90.79
N3-Fe1-N1′	86.92(4)	86.95(5)	N3-Fe1-N4	90.72
N3-Fe1-N2′	88.98(4)	89.04(5)	N3-Fe1-N5	89.59
N3-Fe1-N3′	180.00	180.00	N3-Fe1-N6	179.94
N1′-Fe1-N2′	87.00(4)	86.98(5)	N4-Fe1-N5	83.41
N1′-Fe1-N3′	93.08(4)	93.15(5)	N4-Fe1-N6	89.25
N2′-Fe1-N3′	91.02(4)	90.96(5)	N5-Fe1-N6	90.40
Fe1-N3-C40	158.40(9)	158.62(12)	Fe1-N3-C40	150.2
Fe1-N6-C40′	158.40(9)	158.62(12)	Fe1-N6-C40′	150.3
Σ[b] (°)	28.4	28.5	Σ[b] (°)	35.9

[a] Bond lengths and angles for **1C$_{10}$·140K** are calculated using the average values obtained from the equivalent atoms across the four independent Fe(II) centres in this structure. [b] Octahedral distortion parameters are obtained using the equation: $\Sigma = \sum_{i=1}^{12}(|90-\theta_i|)$, ($\theta_i$ = N-Fe-N) where perfect octahedrons produce a value Σ = 0° and deviation from this value coincides with structural deformation of the coordination polyhedron.

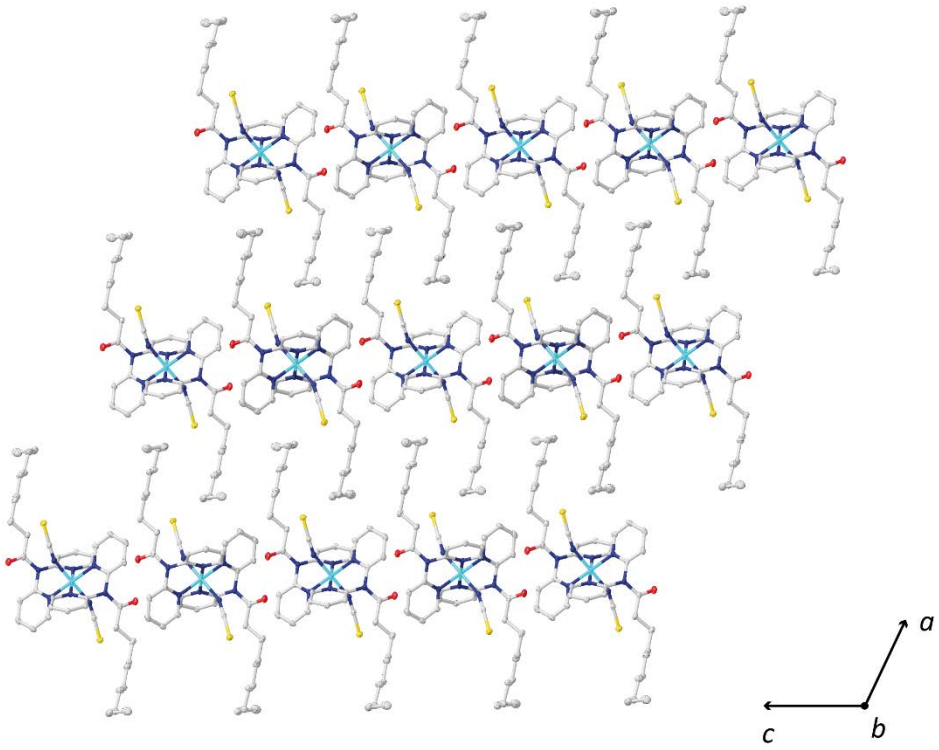

Fig. 5 Packing of **1C$_{10}$·105K** as viewed down the *b* axis. Hydrogen atoms omitted for clarity. Legend: iron, turquoise; nitrogen, blue; carbon, grey; oxygen, red; sulfur, yellow.

Table 6 Selected intermolecular contact distances for **1C$_{10}$**.

	1C$_{10}$·85K	**1C$_{10}$·105K**	**1C$_{10}$·140K**
$\pi\cdots\pi$ (Å)[a]	3.5670(10)	3.5770(13)	3.633(3)
O···C (Å)[b]	3.115(1)	3.121(2)	3.149(7)
O···H-C (°)[b]	130.20(7)	130.37(9)	126.1(3)
Fe···Fe (Å)[c]	8.2351(2)	8.2544(3)	8.5352(7)
Fe···Fe (Å)[d]	15.1219(6)	15.1476(13)	15.1808(12)

[a] Minimum contact distances between intermolecular pyridyl moieties taken between centroids. [b] Shortest interatomic O···C contacts between nearby carbonyls and pyridyl rings. [c] Minimum contact distance between Fe atoms. [d] Shortest Fe···Fe contacts between molecules in parallel 2D networks separated by alkyl chain regions.

The only significant difference between the LS (**1C$_{10}$·85K** and **1C$_{10}$·105K**) and HS (**1C$_{10}$·140K**) structures are the larger interatomic distances associated with the $\pi\cdots\pi$ contacts, C-H···O contacts and Fe···Fe distances, which are larger in **1C$_{10}$·140K** than in **1C$_{10}$·105K** and **1C$_{10}$·85K** as expected (Table 6). In **1C$_{10}$·85K** and **1C$_{10}$·105K** the 2D networks of LS Fe(II) centres are separated by alkyl chains along the *a* axis (Figs. S10 and S11), however in **1C$_{10}$·140K**, these networks propagate perpendicular to the *a* axis and are separated diagonally across the *bc* plane (Figs. S12 and S13). Apart from the orientation of the 2D sheets of complexes and the direction of their alkyl chain tails with respect to the crystallographic axes, the LS and HS structures of **1C$_{10}$** pack identically.

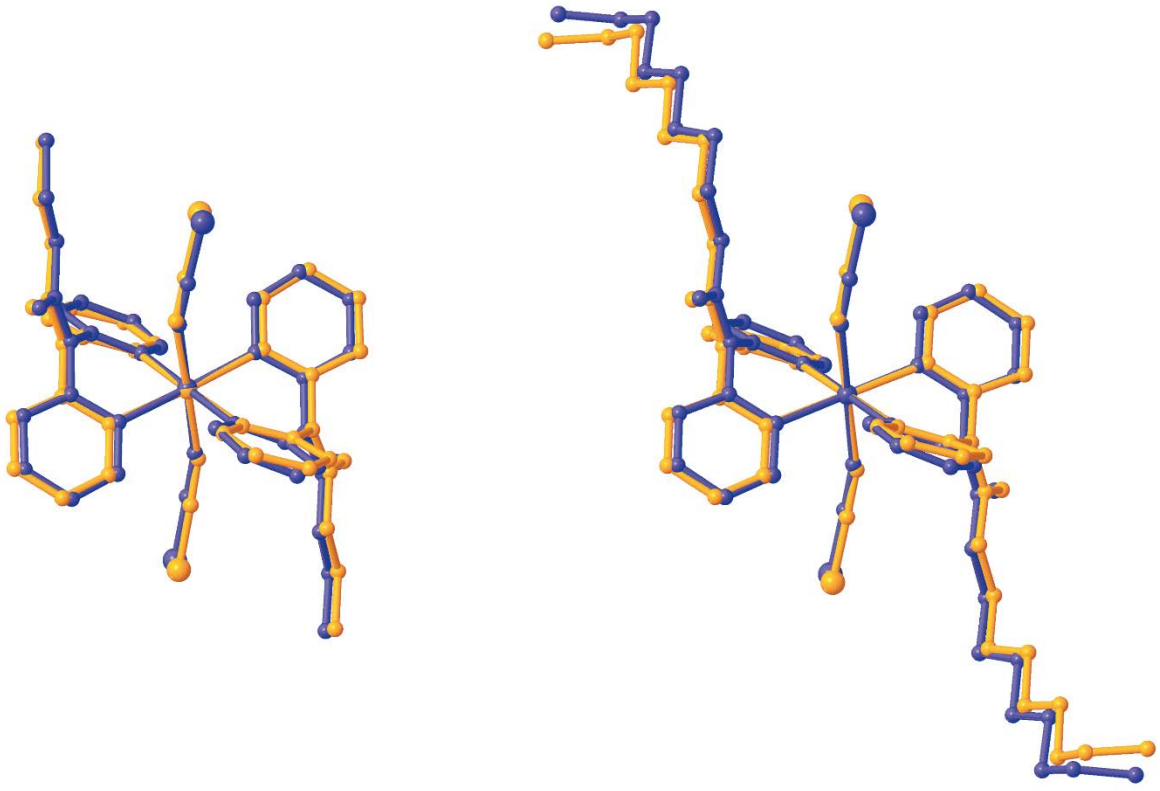

Fig. 6 Overlay of the HS (orange) and LS (blue) molecular structures of **1C$_4$** (left) and **1C$_{10}$** (right). Hydrogen atoms omitted for clarity. Structures were overlaid using the atomic coordinates of the FeN_6 cores in Olex2.[31,32]

For LS **1C$_{10}$·105K** the Fe-N-C angles of the coordinated NCS^- anion are 158.62(12)°, whereas for HS **1C$_{10}$·140K** these angles decrease to an average of 150.2° across all the Fe(II) centres in the asymmetric unit. These changes in the Fe-NCS angles of *trans* isomers are in-line with the observations in **1C$_4$** and are in agreement with the analysis of *trans*-[Fe^{II}(Rdpt)$_2$(NCX)$_2$] complexes (Rdpt = 4-(R)-3,5-di(2-pyridinyl)-4H-1,2,4-triazole, X = S, Se or BH_3) performed by Rodríguez-Jiménez and Brooker.[37] Although there may be a relationship between the Fe-NCS angle and the spin state or even the SCO activity of the heteroleptic complexes of this sort, it remains unclear whether this is applicable to all systems with the general formula *cis*/*trans*-[Fe^{II}(Rdpa)$_2$(NCX)$_2$]. The following coordination compounds: *trans*-[Fe(bdpp)(NCS)$_2$] (bdpp = bis(2',2''-dipyridylamine)pyrimidine),[42] *cis*-[Fe^{II}(DDE)$_2$(NCSe)$_2$] (DDE = N^2,N^2,N^4,N^4-tetraethyl-N^6,N^6-di(pyridin-2-yl)-1,3,5-triazine-2,4,6-triamine),[43] *trans*-[Fe^{II}(DPPyT)(NCS)$_2$] and *trans*-[Fe^{II}(DPPyT)(NCSe)$_2$] (DPPyT = 1-[4,6-bis(dipyridin-2-ylamino)-1,3,5-triazin-2-yl]pyridin-4(1*H*)-one)[14] do not show a consistent decrease in the Fe-NCX angles with the transition from LS to HS in these SCO-active complexes. This suggests that the distortion of the Fe-NCS angles in **1C$_4$** and **1C$_{10}$** between the LS and HS states may be relevant only to the systems reported here. The changes in the molecular structure of **1C$_{10}$** between the LS $P2_1/c$ and HS $P\bar{1}$ crystal structures are subtle and are observed mainly in some slight ligand distortion as well as a slight "bending" of the alkyl chain tails towards the equatorial sites (Fig. 6).

Overall it is clear from the variable temperature crystallographic studies that both complexes undergo a spin-transition between 85 K and 120 K for **1C$_4$** and between 105 K and 140 K for **1C$_{10}$**. In the case of **1C$_{10}$** this is accompanied by a crystallographic phase transition as evidenced by the change of space group from $P2_1/c$ to $P\bar{1}$.

Magnetic studies

From the crystallographic data is it clear that we would expect a spin-transition between 85 K and 120 K for **1C$_4$** and between 105 K and 140 K for **1C$_{10}$**. To confirm this variable temperature magnetic susceptibility measurements were obtained on single crystals of **1C$_4$** and **1C$_{10}$** down to 50 K at a heating/cooling rate of 5 K min^{-1} in an applied DC field of 0.1 T (Fig. 7). The single crystals were removed from the mother liquor and dried in air momentarily before being analysed so that oxidation or decomposition was minimised. Upon cooling from 300 K, **1C$_4$** has a $\chi_M T$ value of 3.50 cm^3 mol^{-1} K down to 175 K, corresponding to a fully HS Fe(II) system. Below 175 K the $\chi_M T$ value decreases slightly to *ca*. 3.30 cm^3 mol^{-1} K at 150 K before a small plateau region is established down to 140 K. An abrupt spin transition then occurs between 140 and 100 K as the value of $\chi_M T$ decreases from 3.25 to 0.13 cm^3 mol^{-1} K, which signifies an almost quantitative LS population of Fe(II) centres. The value of $\chi_M T$ then subtly decreases to 0.09 cm^3 mol^{-1} K at 50 K. To check for thermal hysteresis, the samples were then reheated from 50 K. Upon heating, the $\chi_M T$ value rises gradually, reaching 0.45 cm^3 mol^{-1} K at 122 K. An abrupt spin transition then occurs between 122 and 146 K and the value of $\chi_M T$ reaches 3.22 cm^3 mol^{-1} K. This value increases to 3.51 cm^3 mol^{-1} K at 200 K where it plateaus and the HS state is restored (Fig. 7 top). The SCO in **1C$_4$** is consistent with the crystallographic studies (see above) and shows thermal hysteresis with $\downarrow T_{1/2}$ = 121 K and $\uparrow T_{1/2}$ = 134 K, giving a thermal hysteresis width (ΔT) of 13 K. The observation of thermal hysteresis in **1C$_4$** is surprising as the single crystal structure does not show a temperature-dependent crystallographic phase change from *Pna*2$_1$, which often accompanies thermal hysteresis in the SCO transition temperature ($T_{1/2}$).[40] However, it is possible that the hysteresis in this instance is a collective response due to long-range elastic interactions.

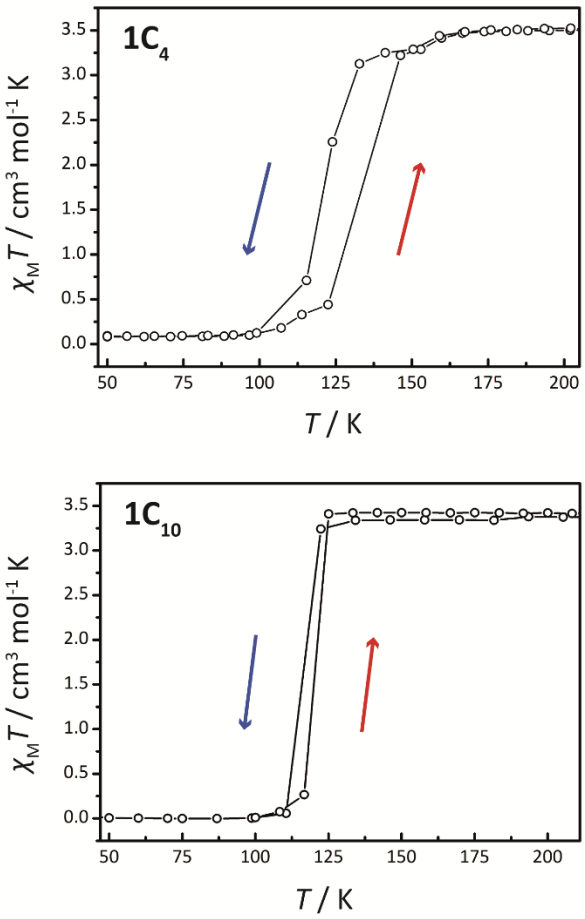

Fig. 7 $\chi_M T$ vs. T plots for single crystals of **1C$_4$** and **1C$_{10}$** at a heating rate of 5 K min^{-1} in a 0.1 T external DC field. The red arrow indicates the heating direction and the blue arrow the cooling direction.

1C$_{10}$ has a $\chi_M T$ value of 3.37 cm^3 mol^{-1} K at 200 K which is expected of a HS Fe(II) system. The value of $\chi_M T$ then decreases slightly to 3.24 cm^3 mol^{-1} K at 123 K before abruptly decreasing to 0.05 cm^3 mol^{-1} K at 111 K. A plateau region is then observed down to 50 K with $\chi_M T$ stabilised at 0.01 cm^3 mol^{-1} K. The sample was then heated from 50 K, and the value of $\chi_M T$ gradually increases to 0.26 cm^3 mol^{-1} K by 116 K before abruptly increasing to 3.42 cm^3 mol^{-1} K at 125 K. The fully HS system is then stable beyond this temperature (Fig. 7 bottom). The SCO in **1C$_{10}$** is thermally hysteretic as was the case with **1C$_4$**, although the width of the

hysteresis is smaller in the former. For **1C$_{10}$** $\downarrow T_{1/2}$ = 117 K and $\uparrow T_{1/2}$ = 121 K, giving ΔT = 4 K, which is 9 K smaller than the 13 K observed in **1C$_4$**. The hysteretic behaviour in **1C$_{10}$** aligns well with the observation of symmetry breaking in the single crystal structures between 105 and 140 K, which correspond to completely LS ($P2_1/c$) and HS ($P\bar{1}$) systems, respectively, on the $\chi_M T$ vs. T plot.

Infrared spectroscopy

Infrared spectra for **1C$_4$**, **1C$_{10}$,** LC$_4$ and LC$_{10}$ can be found in Figs. S14-S16. Infrared spectroscopy was conducted at room temperature on single crystals of **1C$_4$** and **1C$_{10}$**.Both complexes **1C$_4$** and **1C$_{10}$** contain axial thiocyanate ligands which produce characteristic nitrile absorption bands that occur within two distinct regions depending on the spin state of the central Fe(II) ion due to the vibrational differences between electronic states. For Fe(II) the LS $^1A_{1g}$ and HS $^5T_{2g}$ ground electronic states are vibrationally discrete, where the longer coordination bonds of the HS species produce weaker bond force constants, thus oscillating at lower frequencies.[44–46] For Fe(II) species, the nitrile stretch usually appears at *ca*. 2107 cm^{-1} for the LS $^1A_{1g}$ state and between 2040-2070 cm^{-1} for the HS $^5T_{2g}$ state.[47] Both **1C$_4$** and **1C$_{10}$** exhibit strong IR absorption bands at 2043 and 2046 cm^{-1}, respectively, confirming the HS state of both **1C$_4$** and **1C$_{10}$** at room temperature consistent with both the crystallographic and magnetic studies.

UV-vis spectroscopy

Acetone solutions of **1C$_4$** and **1C$_{10}$** rapidly oxidise in atmospheric conditions which is observed as a colour change in solution from yellow to red. This occurs visibly over a matter of minutes and so the Fe(II) species was not stable for a long enough period of time for it to be detected in the UV-visible spectra. **1C$_4$** and **1C$_{10}$** exhibit identical UV-vis properties in solution (Fig. S17),

with slight deviations in molar extinction coefficient (ε) values, which may be due to solid particulates remaining in solution as a consequence of the need to quickly measure the samples after forming the solutions. In acetone, **1C$_4$** and **1C$_{10}$** exhibit two main absorption bands that are not observed in the spectrum for the ligands LC_4 and LC_{10}. These bands have λ_{max} values of 405 and 515 nm (Fig. S17). The band at 515 nm has a molar extinction coefficient value (ε) of 131 $dm^3\ mol^{-1}\ cm^{-1}$ for **1C$_4$** and 107 $dm^3\ mol^{-1}\ cm^{-1}$ for **1C$_{10}$**. The relatively low value of ε at 515 nm is suggestive of weak *d-d* transitions originating from a HS Fe(III) species forming in solution. For the band at 405 nm ε = 979 $dm^3\ mol^{-1}\ cm^{-1}$ for **1C$_4$** and 1130 $dm^3\ mol^{-1}\ cm^{-1}$ for **1C$_{10}$** which is likely to be a weak CT process, due to the magnitude of ε far exceeding that which is typical for *d-d* transitions.[37]

Conclusions

Complexes **1C$_4$** and **1C$_{10}$** vary only by the length of their alkyl chain substituents, which has a significant effect on both their structural and magnetic properties. **1C$_4$** undergoes a quasi-stepped, semi-abrupt spin-crossover centred at 127.5 K, accompanied by a non-uniform thermal hysteresis where ΔT = 13 K. **1C$_{10}$** undergoes an abrupt spin-crossover centred at 119.0 K and is also accompanied by a thermal hysteresis (ΔT = 4 K). The crystallographic phase change in **1C$_{10}$** and subsequent symmetry breaking between the LS and HS states is likely to be the cause of the more abrupt spin-crossover in **1C$_{10}$** compared to **1C$_4$**. The inclusion of hydrophobic alkyl chain substituents on Fe(II) complexes did not inhibit spin-crossover behaviour, but rather demonstrated high cooperativity which resulted in hysteretic and abrupt thermal spin-crossover in the solid state. This is an encouraging sign for future development of multifunctional materials that might rely on alkyl chains for the incorporation

of secondary functionalities such as liquid crystal properties or low-melting point spin-crossover liquids.

Acknowledgements

We thank the EPSRC UK National Crystallography Service at the University of Southampton for the collection of the crystallographic data.[48] IAG and BLG thanks the University of Brighton for a PhD studentship award.

References

1 M. A. Halcrow, *Chem. Soc. Rev.*, 2011, **40**, 4119–4142.

2 M. A. Halcrow, *Chem. Lett.*, 2014, **43**, 1178–1188.

3 K. Boukheddaden, M. H. Ritti, G. Bouchez, M. Sy, M. M. Dîrtu, M. Parlier, J. Linares and Y. Garcia, *J. Phys. Chem. C*, 2018, **122**, 7597–7604.

4 N. Moliner, A. B. Gaspar, M. C. Muñoz, V. Niel, J. Cano and J. A. Real, *Inorg. Chem.*, 2001, **40**, 3986–3991.

5 M. Marchivie, P. Guionneau, J.-F. Létard and D. Chasseau, *Acta Crystallogr. Sect. B*, 2005, **61**, 25–28.

6 C. Lefter, R. Tan, J. Dugay, S. Tricard, G. Molnár, L. Salmon, J. Carrey, W. Nicolazzi, A. Rotaru and A. Bousseksou, *Chem. Phys. Lett.*, 2016, **644**, 138–141.

7 Y. N. Shvachko, D. V Starichenko, A. V Korolyov, A. I. Kotov, L. I. Buravov, V. N. Zverev, S. V Simonov, L. V Zorina and E. B. Yagubskii, *Magnetochemistry*, 2017, **3**, 9.

8 Y. N. Shvachko, D. V Starichenko, A. V Korolyov, E. B. Yagubskii, A. I. Kotov, L. I. Buravov, K. A. Lyssenko, V. N. Zverev, S. V Simonov, L. V Zorina, O. G. Shakirova and L. G. Lavrenova, *Inorg. Chem.*, 2016, **55**, 9121–9130.

9 T. Jasper-Tönnies, M. Gruber, S. Karan, H. Jacob, F. Tuczek and R. Berndt, *J. Phys. Chem. Lett.*, 2017, **8**, 1569–1573.

10 J. Huang, R. Xie, W. Wang, Q. Li and J. Yang, *Nanoscale*, 2016, **8**, 609–616.

11 T. Miyamachi, M. Gruber, V. Davesne, M. Bowen, S. Boukari, L. Joly, F. Scheurer, G. Rogez, T. K. Yamada, P. Ohresser, E. Beaurepaire and W. Wulfhekel, *Nat. Commun.*, 2012, **3**, 936–938.

12 K. Senthil Kumar and M. Ruben, *Coord. Chem. Rev.*, 2017, **346**, 176–205.

13 A. B. Gaspar, G. Agustí, V. Martínez, M. C. Muñoz, G. Levchenko and J. A. Real, *Inorganica Chim. Acta*, 2005, **358**, 4089–4094.

14 T. M. Ross, B. Moubaraki, D. R. Turner, G. J. Halder, G. Chastanet, S. M. Neville, J. D. Cashion, J. Létard, S. R. Batten and K. S. Murray, *Eur. J. Inorg. Chem.*, 2011, 1395–1417.

15 T. M. Ross, B. Moubaraki, S. M. Neville, S. R. Batten and K. S. Murray, *Dalt. Trans.*, 2012, **41**, 1512–1523.

16 W. Nanthawat, R. Olivier, Y. Sujittra and G. Patrick, *Eur. J. Inorg. Chem.*, 2013, 730–737.

17 Y. Galyametdinov, V. Ksenofontov, A. Prosvirin, I. Ovchinnikov, G. Ivanova, P. Gütlich and W. Haase, *Angew. Chemie Int. Ed.*, 2001, **40**, 4269–4271.

18 M. Seredyuk, A. B. Gaspar, V. Ksenofontov, Y. Galyametdinov, J. Kusz and P. Gütlich, *J. Am. Chem. Soc.*, 2008, **130**, 1431–1439.

19 P. Grondin, D. Siretanu, O. Roubeau, M. F. Achard and R. Clérac, *Inorg. Chem.*, 2012, **51**, 5417–5426.

20 M. Seredyuk, M. C. Muñoz, V. Ksenofontov, P. Gütlich, Y. Galyametdinov and J. A. Real, *Inorg. Chem.*, 2014, **53**, 8442–8454.

21 H. L. C. Feltham, K. Dankhoff, C. J. Meledandri and S. Brooker, *Chempluschem*, 2018, **83**, 582–589.

22 M. Hirtz, A. Oikonomou, T. Georgiou, H. Fuchs and A. Vijayaraghavan, *Nat. Commun.*, 2013, **4**, 2591.

23 M. L. Cortez, A. Lorenzo, W. A. Marmisollé, C. Von Bilderling, E. Maza, L. Pietrasanta, F. Battaglini, M. Ceolín and O. Azzaroni, *Soft Matter*, 2018, **14**, 1939–1952.

24 D. Rosario-Amorin, P. Dechambenoit, A. Bentaleb, M. Rouzières, C. Mathonière and R. Clérac, *J. Am. Chem. Soc.*, 2018, **140**, 98–101.

25 S. Schlamp, B. Weber, A. D. Naik and Y. Garcia, *Chem. Commun.*, 2011, **47**, 7152–7154.

26 S. Schlamp, P. Thoma and B. Weber, *Eur. J. Inorg. Chem.*, 2012, 2759–2768.

27 H. S. Scott, B. Moubaraki, N. Paradis, G. Chastanet, J.-F. Letard, S. R. Batten and K. S. Murray, *J. Mater. Chem. C*, 2015, **3**, 7845–7857.

28 S. Schlamp, C. Lochenie, T. Bauer, R. Kempe and B. Weber, *Eur. J. Inorg. Chem.*, 2015, **2015**, 408–413.

29 W. Zhang, F. Zhao, T. Liu, M. Yuan, Z.-M. Wang and S. Gao, *Inorg. Chem.*, 2007, **46**, 2541–2555.

30 G. M. Sheldrick, *Acta Crystallogr. Sect. C Struct. Chem.*, 2015, **71**, 3–8.

31 O. V. Dolomanov, L. J. Bourhis, R. J. Gildea, J. A. K. Howard and H. Puschmann, *J. Appl. Crystallogr.*, 2009, **42**, 339–341.

32 L. J. Bourhis, O. V Dolomanov, R. J. Gildea, J. A. K. Howard and H. Puschmann, *Acta Crystallogr. Sect. A*, 2015, **71**, 59–75.

33 G. M. Sheldrick, *Acta Crystallogr. Sect. A*, 2008, **64**, 112–122.

34 A. Hauser, in *Spin Crossover in Transition Metal Compounds I*, eds. P. Gütlich and H. A. Goodwin, Springer Berlin Heidelberg, Berlin, Heidelberg, 2004, vol. 233, pp. 49–58.

35 P. Guionneau, M. Marchivie, G. Bravic, J.-F. Létard and D. Chasseau, in *Spin Crossover in Transition Metal Compounds II*, eds. P. Gutlich and H. Goodwin, Springer, Berlin, Heidelberg, Berlin, Heidelberg, 2004, vol. 234, pp. 97–128.

36 P. Guionneau, M. Marchivie, G. Bravic, J.-F. Letard and D. Chasseau, *J. Mater. Chem.*, 2002, **12**, 2546–2551.

37 S. Rodríguez-Jiménez and S. Brooker, *Inorg. Chem.*, 2017, **56**, 13697–13708.

38 G. R. Desiraju, *Acc. Chem. Res.*, 1996, **29**, 441–449.

39 G. R. Desiraju, *Acc. Chem. Res.*, 1991, **24**, 290–296.

40 M. Shatruk, H. Phan, B. A. Chrisostomo and A. Suleimenova, *Coord. Chem. Rev.*, 2015, **289**–**290**, 62–73.

41 W. Phonsri, C. G. Davies, G. N. L. Jameson, B. Moubaraki, J. S. Ward, P. E. Kruger, G. Chastanet and K. S. Murray, *Chem. Commun.*, 2017, **53**, 1374–1377.

42 S. M. Neville, B. A. Leita, G. J. Halder, C. J. Kepert, B. Moubaraki, J.-F. Létard and K. S. Murray, *Chem. Eur. J.*, 2008, **14**, 10123–10133.

43 T. M. Ross, B. Moubaraki, K. S. Wallwork, S. R. Batten and K. S. Murray, *Dalt. Trans.*, 2011, **40**, 10147–10155.

44 S. Mebs, B. Braun, R. Kositzki, C. Limberg and M. Haumann, *Inorg. Chem.*, 2015, **54**, 11606–11624.

45 M. Sorai and S. Seki, *J. Phys. Chem. Solids*, 1974, **35**, 555–570.

46 M. Sorai, J. Ensling and P. Gütlich, *Chem. Phys.*, 1976, **18**, 199–209.

47 R. G. Miller and S. Brooker, *Chem. Sci.*, 2016, **7**, 2501–2505.

48 S. J. Coles and P. A. Gale, *Chem. Sci.*, 2012, **3**, 683–689.